

Research Paper

# Vibrations of Multi-Layer Beam with Nanocomposite Face Sheets Reinforced with Graphene Platelets and Porous Core

A. Mihankhah<sup>1</sup>, Z. Khoddami Maraghi<sup>2</sup>, A. Ghorbanpour Arani<sup>1,3\*</sup>, Sh. Niknejad<sup>1</sup>

<sup>1</sup>Faculty of Mechanical Engineering, University of Kashan, Kashan, Iran

<sup>2</sup>Faculty of Engineering, Mahallat Institute of Higher Education, Mahallat, Iran

<sup>3</sup>Institute of Nanoscience and Nanotechnology, University of Kashan, Kashan, Iran

Received 30 March 2023; accepted 26 May 2023

## ABSTRACT

The current article investigates the free vibrations of a three-layer beam. The middle layer of this structure is selected from porous material. For modeling the porous layer, linear pro-elasticity relationships are applied, while Young's modulus and its density vary along the thickness. The upper and lower layers of the structure are reinforced with graphene nanoplates and can take different configurations as Parabolic, linear, and uniform. In this study, with the help of Halpin-Tsai modified theory, equivalent composite coefficients will be extracted. The equations of motion in three layers are derived with the help of third order shear theory, energy method and Hamilton's Principle. Among the significant results of this article, we can mention the effect of amplifiers in improving the vibration behavior of the beam, the effect of pore pressure and volume fraction of reinforcement on the frequency of vibrations. The results of this research can be applied in marine, aerospace, and civil industries.

© 2023 IAU, Arak Branch. All rights reserved.

**Keywords :** Vibration; Three-layer beam; Graphene nanoplatelets reinforced composites; Porous materials.

## 1 INTRODUCTION

IN the last 30 years, the use of composite materials has been grown strikingly in different industries. Initially, this use was limited to the aerospace industry, but with the passage of time and the emergence of newer and cheaper materials and stunning developments in the field of composite material manufacturing technologies, the use of these materials in common industries such as automotive, shipbuilding, transportation a rail transportation, industries related to the energy sector and many other industries grew. The most important reason for the growth of the use of these materials was the desire of manufacturers to reduce weight along with increasing the strength and safety of their products. The sensitivity of this issue shows itself especially in the aerospace industry, where the issue of weight is one of the fundamental issues of these industries. In addition to the discussion of the high strength-to-weight ratio of these materials, their good thermal and insulating properties and the acoustic issues, resistance to

\*Corresponding author. Tel.: +98 31 55912450; Fax: +98 31 55912424.  
E-mail address: aghorban@kashanu.ac.ir (A.Ghorbanpour Arani)

fatigue and accurate and easy plasticity are potentially vital in the aerospace industry, so these materials are very good alternatives for common metals used in industries. In the meantime, sandwich structures have been widely used in various industries in the last few years due to their lightness and high hardness. One of the most privileged uses of these structures is in aircraft bodies, ship structures and wind turbine blades. On the other hand, carbon and its derivatives can be considered as effective reinforcements in order to promote the thermomechanical performance of composite structures. Since the last decades, carbon fiber (CF) has been used on a large scale in numerous applications. With the help of advanced production process in industries, a new class of composites reinforced with nanoparticles were introduced. An obvious improvement in the mechanical performance of structures was reported as a result of using nanofibers instead of macroscale fibers. Therefore, the investigation of the mechanical behavior of Carbon Nanotube-Reinforced (CNTR) attracted a lot of attention as a famous carbon-based nanofiber [1]. The mechanics of porous media is a branch of physics that studies the behavior of porous materials saturated with a fluid such as water. In other words, a porous material is one that contains a continuous network of pores that is filled by water or another fluid. As mentioned earlier, many natural materials such as soil or body tissues such as bone cartilage, and muscle exemplify porous materials. Regarding each of the mentioned groups several articles have been published, so an effort has been made to introduce some of them in this section. Choi et al [2] studied the mechanical properties of composite beams of electrorheological fluids in the state of free vibrations. They also considered the effects of electrorheological fluid and applied electric field on the composite modulus of the structure. Sandwich beams are used in various engineering applications due to their high strength. Modeling and vibration analysis of viscoelastic sandwich beams have been studied in many types of research. Many efforts have been made to restrain electrorheological fluids in various structures in order to reduce their vibration problems. To this end, extensive studies have been conducted in the field of analyzing the mechanical behavior of sandwich structures with a core made of electrorheological materials. Yeh et al [3] investigated the dynamic stability of a sandwich beam with an electrorheological core under a dynamic axial load. They used the finite element and harmonic balance methods to obtain the dynamic response of the sandwich beam and concluded that the electrorheological core has a very significant effect on the dynamic stability region of the sandwich structure. Wei et al [4] analyzed the features of vibrations in a rotating sandwich beam with an electrorheological core. They obtained the stress-strain relations for an electrorheological material according to its complex bulk modulus and with the help of the theory of linear viscoelasticity. The nonlinear equations of motion were extracted by using Hamilton's principle and investigated by applying the finite element method. In this research, they reported the effect of parameters such as electric field intensity and beam rotation speed on natural frequency and loss coefficient. Their findings illustrated a noticeable decrease in vibrations at different rotation speeds of the beam with increasing electric field intensity. Furthermore, they claimed that such a system can be used to control the vibrations of rotating beams. The vibration analysis of sandwich beams with electrorheological core was studied by Allahvardizade et al [5]. They applied Timoshenko's beam theory to model the structure and obtain the equations of motion and finally found the effects of the thickness of the layers and the applied electric field on the natural frequencies of the beam. Rezaei Pazhand and Pahlavan [6] studied the transient response of a three-layer beam containing an electrorheological fluid. They found that when the electric field is applied to the beam, its dynamic characteristics change, so that this characteristic can be used to suppress vibrations and reduce the settling time in such instruments. They used finite element method and direct integral algorithm to simulate the impact response in sandwich beam. In order to investigate the natural frequency and settling time, they simulated the electrorheological fluid with the Bingham plastic model and showed the effect of different thickness ratios by applying different electric fields on it. Ramkoulmar and Gansan [7] investigated the vibrations and damping of a composite sandwich column with a rectangular and hollow section. They used electro-rheological fluid as a viscoelastic layer in this structure. Modal strain energy and finite element methods were used to predict the loss coefficient and frequency of composite sandwich layers. In this research, the effect of parameters such as core thickness, fiber angle in composite layers, applied voltage and arrangement of layers under clamped-free boundary condition on sheet vibration frequency were studied. Few number of studies conducted on sandwich beams have investigated the mechanical behavior of the beam with a core made of electrorheological materials covered by functional graded layers. Accordingly, Asgari and Kouchzade [8] investigated the instability of a three-layer sandwich beam with a rectangular cross-section. They chose the beam core from magnetorheological fluid. The formulation of the problem was based on the classical thin shell theory for the upper and lower layers. They did research on the effects of applied magnetic field, thickness of the core and layers containing the core on the critical aerodynamic pressure for different boundary conditions. In the end, they concluded that the intensity of the magnetic field and the thickness ratio have considerable effects on the instability of the sandwich beam. wave propagation and vibration of a porous beam embedded via nanocomposite piezoelectric layers were investigated by Keshtegar et al [9]. The nonlinear free vibration behavior of shear deformable sandwich porous beam is investigated in this paper within the context of Timoshenko beam theory by

Chen et al [10]. They discussed the effects of porosity coefficient, slenderness ratio, thickness ratio, and boundary conditions. Asemi et al [11]. investigated static, dynamic and natural frequency analyses of functionally graded porous annular sector plate reinforced by graphene nanoplatelets. They derived Hamilton's principle based on first shear deformation plate theory and finite element method. Their results showed different distribution of porosity, porosity coefficient, GPL dispersion patterns, and weight fraction of GPL nanofiller, boundary conditions and sector angles on natural frequency, static and transient responses of the plate. Kiarasi et al [12]. Examined a high demand for great structural implementation and multifunctionality with excellent mechanical properties. They reviewed (a) briefly reviewed the mechanical properties of functionally graded porous composites reinforced by GPLs and discusses the existing micromechanics model for the prediction of effective mechanical properties; (b) presented a comprehensive review on the mechanical analyses of these structures; (c) discussed the challenges and possible future works. Kiarasi et al [13]. investigated Natural frequency analysis of functionally graded porous joined truncated conical–cylindrical shell reinforced by graphene platelet. They conducted he effects of different geometric parameters, boundary conditions, weight fraction of graphene platelets, porosity coefficient, distribution of porosity and dispersion pattern of graphene platelets on the natural frequencies and mode shapes of the structure. Babaei et al [14]. investigated dynamic behavior of functionally graded saturated porous rotating thick truncated cone. Their results demonstrated by increasing Skempton coefficient, natural frequencies are increased, and natural frequencies of PUD distribution are lower than other distributions. Also, rotational velocity and semi-vertex angle have significant effect on the displacement and stress field.

This article focuses on 3 main topics for vibration analysis.

- The beam structure is selected for vibration analysis. three beam theories (Euler, Timoshenko, and Reddy) are used, and the results are compared together.
- Graphene nanoplatelets (GNPs) are novel nanofillers that are applied to reinforce the up and button layers. Graphene nanoplatelets reinforced composites (GNPLRC) have been used in this research. Graphene nanoplatelets (GNPs) are novel nanofillers that have attractive properties, including strong compatibility with most polymers, high strength, and economic efficiency
- symmetric, and nonsymmetric porous materials are used for inter-layer.

According to this, parameters such as the thickness of the layers and the length of the beam, different vibrational modes, porosity, holes distribution pattern, and mass fraction of graphene nanoplatelets are investigated.

## 2 MATHEMATICAL MODELING

The figure below shows a beam with three layers in length. The upper and lower layers are made of graphene nanoplatelets reinforced composites and the core is made of porous material.

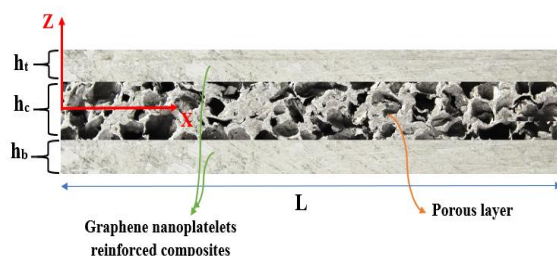


**Fig.1**  
Schematic figure of the Beam.

In this article, ESL theories are applied, in which the set of composite layers is assumed to be an equivalent single layer and the kinematic relations of displacement are considered for it. These types of theories turn a three-dimensional problem into a two-dimensional problem. In contrast, there are three-dimensional theories that assume each layer as a separate three-dimensional object. The main purpose of this research is to investigate the overall free vibrations of the beam.

Accordingly, the three layers of the mentioned beam with the same displacements of different materials are considered as follows:

1. Upper and lower layers of composite reinforced with graphene nanoplatelets
2. Middle layer of porous material.

Next, the stress-strain relations related to the material of each layer are rewritten.

### 3 CORE MODELING

As assumed in the previous sections, the innovation of this research is that the core is made of porous material which is shown in Figs (1-3). The behavior of porous media such as porosity, twisting, shape and composition of materials, which are entered at higher levels, but are ignored in linear mode. The displacement strain equations for fluids are generally obtained as follows [15]:

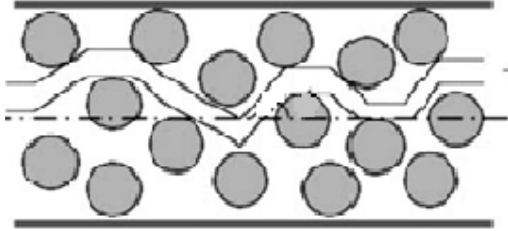


**Fig.2**  
Schematic Figure of Porous Core Saturated [15].

According to Hooke's law, the strain of porous materials are obtained with  $Q_{11} = \frac{E_z}{1-\nu^2}$  when the porous core is uniform as:

$$E(z) = E_1(1 - e_0 a) \quad (1)$$

$$\rho(z) = \rho_1 \sqrt{(1 - e_0 a)} \quad (2)$$

$$a = \frac{1}{e_0} - \frac{1}{e_0} \left( \frac{2}{\pi} \sqrt{(1 - e_0)} - \frac{2}{\pi} + 1 \right)^2 \quad (3)$$

And for symmetric porous core:

$$E(z) = E_1 \left( 1 - e_0 \cos \left( \frac{\pi z}{h_c} \right) \right) \quad (4)$$

$$\rho(z) = \rho_1 \left( 1 - e_m \cos \left( \frac{\pi z}{h_c} \right) \right) \quad (5)$$

And for Non-symmetric porous core:

$$E(z) = E_1 \left( 1 - e_0 \cos \left( \frac{\pi z}{h_c} + \frac{\pi}{4} \right) \right) \quad (6)$$

$$\rho(z) = \rho_1 \left( 1 - e_m \cos \left( \frac{\pi z}{h_c} + \frac{\pi}{4} \right) \right) \quad (7)$$

### 4 STRUCTURAL EQUATIONS OF NANOCOMPOSITE LAYERS

The layers of this structure consist of the background matrix and nanoplatelets made of graphene. After calculating the strain to obtain the corresponding stresses, the relationship between the strain and stress according to Hooke's law is as follows, in which the vertical stress in the Z direction can be ignored and can be converted into a two-dimensional matrix:

$$\begin{bmatrix} \sigma_x \\ \sigma_z \\ \tau_{xz} \end{bmatrix} = \begin{pmatrix} C_{11} & C_{13} & 0 \\ C_{13} & C_{33} & 0 \\ 0 & 0 & C_{55} \end{pmatrix} \begin{Bmatrix} \varepsilon_{xx} \\ \varepsilon_{zz} \\ \gamma_{xz} \end{Bmatrix} \tag{8}$$

$$\begin{bmatrix} \sigma_x \\ \tau_{xz} \end{bmatrix} = \begin{pmatrix} C_{11} & 0 \\ 0 & C_{55} \end{pmatrix} \begin{Bmatrix} \varepsilon_{xx} \\ \gamma_{xz} \end{Bmatrix}$$

where in the composite reference books [16]:

$$C_{11} = C_{33} = \frac{E}{1-\nu^2}, \quad C_{55} = G_m, \quad C_{13} = \nu C_{11} \tag{9}$$

The mechanical properties of the layers are also different according to their thickness. To determine the effective values of these features, among different models, Halpin-Tsai micromechanical models and mixture law have been used to obtain these features. Halpin-Tsai micromechanical model paves the way for the following relationship to predict the effective value of Young's modulus [17].

$$E(z) = \frac{3}{8} \left( \frac{1 + \zeta_L \eta_L V_{GPL}}{1 - \eta_L V_{GPL}} \right) E_M + \frac{5}{8} \left( \frac{1 + \zeta_W \eta_W V_{GPL}}{1 - \eta_W V_{GPL}} \right) E_M \tag{10}$$

$$\zeta_L = 2 \left( \frac{L_{GPL}}{h_{GPL}} \right), \tag{11}$$

$$\zeta_W = 2 \left( \frac{w_{GPL}}{h_{GPL}} \right), \tag{12}$$

$$\eta_W = \left[ \left( \frac{E_{GPL}}{E_M} \right) - 1 \right] / \left[ \left( \frac{E_{GPL}}{E_M} \right) + \zeta_W \right], \tag{13}$$

$$\eta_L = \left[ \left( \frac{E_{GPL}}{E_M} \right) - 1 \right] / \left[ \left( \frac{E_{GPL}}{E_M} \right) + \zeta_L \right] \tag{14}$$

$L_{GPL}$  shows the length of nanographenes, their thickness is shown by  $h_{GPL}$  and their width is shown by  $w_{GPL}$ . In addition,  $E_{GPL}$  is the Young's modulus for strengthening graphenes. It should be taken into consideration that the sum of the volume fractions of GPL and matrix is equal to one and their sum is obtained through the following equation [17]:

$$V_{GPL} = \frac{g_{GPL}(z)}{g_{GPL}(z) + \left( \frac{\rho_{GPL}}{\rho_M} \right) (1 - g_{GPL}(z))} \tag{15}$$

In the above relationship,  $\rho$  is the density and also,  $g_{GPL}$  refers to the weight fraction of the reinforcements, which is as follows for the three dispersion patterns considered [17]:

$$g_{GNP}(z) = \begin{cases} g_{GNP}^* & \text{Uniform} \\ \left[1 - \frac{2z}{h_f}\right] g_{GNP}^* & \text{FG-A} \\ \left[1 + \frac{2z}{h_f}\right] g_{GNP}^* & \text{FG-V} \\ 2 \left[1 - \frac{2z}{h_f}\right] g_{GNP}^* & \text{FG-O} \\ \frac{4|z|}{h_f} g_{GNP}^* & \text{FG-X} \end{cases}, \quad g_{GNP}^* = 0.01 \quad (16)$$

where  $h_f$  is the thickness of upper and lower layers. Other characteristics of the upper layer include Poisson's ratio and density according to the law of mixture as follows [17]:

$$\rho(z) = \rho_{GPL} V_{GPL} + \rho_M V_M, \quad (17)$$

$$\nu(z) = \nu_{GPL} V_{GPL} + \nu_M V_M \quad (18)$$

$V_{GPL}$  and  $V_M$  are the Poisson's ratio of the background matrix and nanographenes.

## 5 BEAM THEORY

Different theories related to beams in deformation kinematics currently exist and are used. To explain the beam theories, the coordinate system must be described first. The axis in the longitudinal direction of the beam, the axis in the direction of the thickness (maximum thickness) and the axis in the transverse direction of the beam are taken into consideration. In general, in a beam theory, all applied loads and geometry are only a function of the coordinates, as are the displacements along the coordinates. It is assumed that the displacement is exactly zero.

In this article, for a better understanding and comparison of first order and high order theories according to formula (1-1), the following general theory is applied.

$$u(x, z, t) = u_0(x, t) - f(z) \frac{\partial w_0(x, t)}{\partial x} + g(z) \varphi_0(x, t), \quad w(x, z, t) = w_0(x, t) \quad (19)$$

$w_0$  and  $u_0$  are the in-plane displacement and vertical displacement in the  $x$  and  $z$  directions, respectively.  $F(z)$  and  $g(z)$  are also the defining function of the beam theory [18].

$$\begin{aligned} \left. \begin{aligned} f(z) &= 0 \\ g(z) &= z \end{aligned} \right\} \longrightarrow \text{Timoshenko} \\ \left. \begin{aligned} f(z) &= z \\ g(z) &= 0 \end{aligned} \right\} \longrightarrow \text{Euler} \\ \left. \begin{aligned} f(z) &= C_1 z^3 \\ g(z) &= z - C_1 z^3 \end{aligned} \right\} \longrightarrow \text{Reddy } (C_1 = \frac{4}{3h^2}) \end{aligned} \quad (20)$$

The kinematic relations of the procedures are stated, and the displacement strain relations for the beam in the linear range are as follows [19]:

$$\varepsilon_{xx} = \frac{\partial u(x, z, t)}{\partial x}, \quad \varepsilon_{zz} = \frac{\partial w(x, z, t)}{\partial z}, \quad \gamma_{xz} = \frac{\partial u(x, z, t)}{\partial z} + \frac{\partial w(x, z, t)}{\partial x} \quad (21)$$

By replacing relation (1-3) in relation (3-2), the strain components can be expressed as follows:

$$\begin{aligned} \varepsilon_{xx} &= \frac{\partial u_0(x,t)}{\partial x} - f(z) \left( \frac{\partial^2 w_0(x,t)}{\partial x^2} \right) + g(z) \left( \frac{\partial \varphi(x,t)}{\partial x} \right) \\ \varepsilon_{zz} &= 0 \\ \gamma_{xz} &= \frac{\partial w_0(x,t)}{\partial x} - f'(z) \frac{\partial w_0(x,t)}{\partial x} + g'(z) \varphi_0(x,t) \end{aligned} \tag{22}$$

## 6 EQUATIONS OF MOTION

Among the various methods used to obtain the equations of motion, the energy method has been applied in this research because of its comprehensiveness. In the energy method, total energy is obtained from the sum of strain energy, kinetic energy and work caused by external loads (in the present work  $W=0$ ) [20].

$$\Pi = U - (T + W) \tag{23}$$

In this research, the strain energy of the whole system is equal to the sum of the strain energy of the layer beam and core model in the structure [21]:

$$U = U_{t,b} + U_c \tag{24}$$

$$U = \frac{1}{2} \int_{-h_c/2-h_b}^{-h_c/2} \int_x (\sigma_x \varepsilon_{xx} + \tau_{xz} \gamma_{xz}) \, dx \, dz + \frac{1}{2} \int_{-h_c/2}^{h_c/2} \int_x \tau_{xz}^c \gamma_{xz}^c \, dx \, dz + \frac{1}{2} \int_{h_c/2}^{h_c/2+h_t} \int_x (\sigma_x \varepsilon_{xx} + \tau_{xz} \gamma_{xz}) \, dx \, dz \tag{25}$$

Kinetic Energy: According to the displacement of the sandwich beam in two directions, the velocities in these two directions are defined and the kinetic energy is written as follows [22]:

$$\begin{aligned} K &= \frac{1}{2} \rho_i \int_0^L \int_A \left[ \left( \frac{\partial u}{\partial t} \right)^2 + \left( \frac{\partial w}{\partial t} \right)^2 \right] dA \, dx \\ K &= \frac{1}{2} \int_{h_c/2}^{h_c/2+h_t} \int_x \rho_t \left[ \left( \frac{\partial u}{\partial t} \right)^2 + \left( \frac{\partial w}{\partial t} \right)^2 \right] dx \, dz + \frac{1}{2} \int_{-h_c/2}^{h_c/2} \int_x \rho_c \left( \frac{\partial w}{\partial t} \right)^2 dx \, dz + \frac{1}{2} \int_{-h_c/2}^{h_c/2} \int_x \rho_c z^2 \left( \frac{\partial \gamma_{xz}^c}{\partial t} \right)^2 dx \, dz \\ &\quad + \frac{1}{2} \int_{-h_c/2-h_b}^{-h_c/2} \int_x \rho_t \left[ \left( \frac{\partial u}{\partial t} \right)^2 + \left( \frac{\partial w}{\partial t} \right)^2 \right] dx \, dz \end{aligned} \tag{26}$$

In this equation,  $\rho_i$  ( $i = t, b, c$ ) represents density. Through using the Eqs. (3-28) and setting the coefficients to zero,  $\delta T_i, \delta U_i$  and the equations of motion for the third layer can be calculated by the following equation:

$$\int_{t_0}^{t_1} [\delta U_i - \delta K_i] \, dt = 0 \tag{27}$$

which  $i = (t, b, c)$  shows for three layers. With the help of Hamilton's principle, the equations of motion of the multilayer beam are derived as follows:

Euler-Bernoulli Beams Theory (EBBT).  
Governing motion equations:

$$\begin{aligned}
\delta u : \\
-Q_{110} \frac{\partial^2}{\partial x^2} u(x,t) + Q_{111} \frac{\partial^3}{\partial x^3} w(x,t) + I_0 \frac{\partial^2}{\partial t^2} u(x,t) - I_1 \frac{\partial^3}{\partial x \partial t^2} w(x,t) = 0, \\
\delta w : \\
-Q_{111} \frac{\partial^3}{\partial x^3} u(x,t) + Q_{112} \frac{\partial^4}{\partial x^4} w(x,t) + I_1 \frac{\partial^3}{\partial x \partial t^2} u(x,t) - I_2 \frac{\partial^4}{\partial x^2 \partial t^2} w(x,t) + I_0 \frac{\partial^2}{\partial t^2} w(x,t) + \Delta P = 0
\end{aligned} \tag{28}$$

Boundary conditions:

$$\begin{aligned}
\left( Q_{110} \frac{\partial}{\partial x} u(x,t) - Q_{111} \frac{\partial^2}{\partial x^2} w(x,t) \right) (\delta u) &= 0, \\
\left( Q_{111} \frac{\partial^2}{\partial x^2} u(x,t) - Q_{112} \frac{\partial^3}{\partial x^3} w(x,t) \right) (\delta w) &= 0, \\
\left( -Q_{111} \frac{\partial}{\partial x} u(x,t) + Q_{112} \frac{\partial^2}{\partial x^2} w(x,t) \right) \left( \frac{\partial \delta w}{\partial x} \right) &= 0
\end{aligned} \tag{29}$$

Coefficient's definitions are presented in Appendix A (A.1).

Reddy's Beams Theory (RBT).

Governing motion equations:

$$\begin{aligned}
\delta u : \\
-Q_{110} \frac{\partial^2}{\partial x^2} u(x,t) + Q_{111} \frac{\partial^3}{\partial x^3} w(x,t) - Q_{112} \frac{\partial^2}{\partial x^2} \phi(x,t) + I_0 \frac{\partial^2}{\partial t^2} u(x,t) - I_1 \frac{\partial^3}{\partial x \partial t^2} w(x,t) + I_2 \frac{\partial^2}{\partial t^2} \phi(x,t) = 0 \\
\delta w : \\
+Q_{111} \frac{\partial^3}{\partial x^3} u(x,t) - Q_{113} \frac{\partial^4}{\partial x^4} w(x,t) + Q_{550} \frac{\partial^2}{\partial x^2} w(x,t) + Q_{553} \frac{\partial^2}{\partial x^2} w(x,t) - 2Q_{551} \frac{\partial^2}{\partial x^2} w(x,t) \\
+Q_{114} \frac{\partial^3}{\partial x^3} \phi(x,t) + Q_{552} \frac{\partial}{\partial x} \phi(x,t) - Q_{554} \frac{\partial}{\partial x} \phi(x,t) - I_1 \frac{\partial^3}{\partial x \partial t^2} u(x,t) - I_0 \frac{\partial^2}{\partial t^2} w(x,t) \\
+I_3 \frac{\partial^4}{\partial x^2 \partial t^2} w(x,t) - I_4 \frac{\partial^3}{\partial x \partial t^2} \phi(x,t) - \Delta P = 0 \\
-Q_{112} \frac{\partial^2}{\partial x^2} u(x,t) + Q_{114} \frac{\partial^3}{\partial x^3} w(x,t) + Q_{552} \frac{\partial}{\partial x} w(x,t) - Q_{554} \frac{\partial}{\partial x} w(x,t) - Q_{115} \frac{\partial^2}{\partial x^2} \phi(x,t) \\
+Q_{555} \phi(x,t) + I_2 \frac{\partial^2}{\partial t^2} u(x,t) - I_4 \frac{\partial^3}{\partial x \partial t^2} w(x,t) + I_5 \frac{\partial^2}{\partial t^2} \phi(x,t) = 0 \\
\delta \phi : \\
-Q_{112} \frac{\partial^2}{\partial x^2} u(x,t) + Q_{114} \frac{\partial^3}{\partial x^3} w(x,t) + Q_{552} \frac{\partial}{\partial x} w(x,t) - Q_{554} \frac{\partial}{\partial x} w(x,t) - Q_{115} \frac{\partial^2}{\partial x^2} \phi(x,t) \\
+Q_{555} \phi(x,t) + I_2 \frac{\partial^2}{\partial t^2} u(x,t) - I_4 \frac{\partial^3}{\partial x \partial t^2} w(x,t) + I_5 \frac{\partial^2}{\partial t^2} \phi(x,t) = 0
\end{aligned} \tag{30}$$

Boundary conditions:

$$\begin{aligned}
 & \left( Q_{110} \frac{\partial}{\partial x} u(x,t) - Q_{111} \frac{\partial^2}{\partial x^2} w(x,t) + Q_{112} \frac{\partial}{\partial x} \phi(x,t) \right) (\delta u) = 0, \\
 & \left( \begin{aligned} & Q_{111} \frac{\partial}{\partial x} u(x,t) - Q_{113} \frac{\partial^2}{\partial x^2} w(x,t) + Q_{114} \frac{\partial}{\partial x} \phi(x,t) + Q_{553} \frac{\partial}{\partial x} w(x,t) \\ & - Q_{554} \phi(x,t) - 2Q_{551} \frac{\partial}{\partial x} w(x,t) + Q_{552} \phi(x,t) + Q_{550} \frac{\partial}{\partial x} w(x,t) \end{aligned} \right) (\delta w) = 0, \\
 & \left( -Q_{111} \frac{\partial}{\partial x} u(x,t) + Q_{113} \frac{\partial^2}{\partial x^2} w(x,t) - Q_{114} \frac{\partial}{\partial x} \phi(x,t) \right) \left( \frac{\partial \delta w}{\partial x} \right) = 0, \\
 & \left( Q_{112} \frac{\partial}{\partial x} u(x,t) - Q_{114} \frac{\partial^2}{\partial x^2} w(x,t) + Q_{115} \frac{\partial}{\partial x} \phi(x,t) \right) (\delta \phi) = 0
 \end{aligned} \tag{31}$$

Coefficient's definitions are presented in Appendix A (A.2).  
 Timoshenko's Beams Theory (TBT).  
 Governing motion equations:

$$\begin{aligned}
 \delta u : \\
 & -Q_{110} \frac{\partial^2}{\partial x^2} u(x,t) - Q_{111} \frac{\partial^2}{\partial x^2} \phi(x,t) + I_0 \frac{\partial^2}{\partial t^2} u(x,t) + I_1 \frac{\partial^2}{\partial t^2} \phi(x,t) = 0, \\
 \delta w : \\
 & \kappa_f Q_{550} \frac{\partial^2}{\partial x^2} w(x,t) + \kappa_f Q_{550} \frac{\partial}{\partial x} \phi(x,t) - I_0 \frac{\partial^2}{\partial t^2} w(x,t) - \Delta P = 0, \\
 \delta \phi : \\
 & -Q_{111} \frac{\partial^2}{\partial x^2} u(x,t) + \kappa_f Q_{550} \frac{\partial}{\partial x} w(x,t) - Q_{112} \frac{\partial^2}{\partial x^2} \phi(x,t) + \kappa_f Q_{550} \phi(x,t) + I_1 \frac{\partial^2}{\partial t^2} u(x,t) + I_2 \frac{\partial^2}{\partial t^2} \phi(x,t) = 0
 \end{aligned} \tag{32}$$

Boundary conditions:

$$\begin{aligned}
 & \left( Q_{110} \frac{\partial}{\partial x} u(x,t) + Q_{111} \frac{\partial}{\partial x} \phi(x,t) \right) (\delta u) = 0, \\
 & \left( \kappa_f Q_{550} \phi(x,t) + \kappa_f Q_{550} \frac{\partial}{\partial x} w(x,t) \right) (\delta w) = 0, \\
 & \left( Q_{111} \frac{\partial}{\partial x} u(x,t) + Q_{112} \frac{\partial}{\partial x} \phi(x,t) \right) (\delta \phi) = 0
 \end{aligned} \tag{33}$$

Coefficient's definitions are presented in Appendix A (A.3).

## 7 SOLUTION BY DQM

DQM is employed which in essence approximates the partial derivative of a function, with respect to a spatial variable at a given discrete point, as a weighted linear sum of the function values at all discrete points chosen in the solution domain of the spatial variable. Let  $F$  be a function representing  $u_i, w_i, \psi_i$  and  $\phi_i$  with respect to variable  $\xi$  in the following domain of  $(0 < \xi < L)$  having  $N_\xi$  grid points along these variable.

The  $n$ th-order partial derivative of  $F(\xi)$  with respect to  $\xi$  may be expressed discretely [23] at the point  $(\xi_i)$  as :

$$\frac{d^n F(\xi_i)}{d\xi^n} = \sum_{k=1}^{N_\xi} A_{ik}^{(n)} F(\xi_k) \quad n = 1, \dots, N_\xi - 1, \quad (34)$$

where is the weighting coefficients associated with  $n$ th-order partial derivative of with respect to at the discrete point whose recursive formulae can be found in. A more superior choice for the positions of the grid points is Chebyshev polynomials as expressed in [23].

Numerical discretization of time-dependent partial equations is divided into two parts, spatial discretization and time discretization. In spatial discretization, many methods are used by researchers, including finite difference, finite component, finite volume, spectral, and differential quadratic methods. Among these methods, the first three methods are considered as low order methods, while spectral and differential quadratic methods are known as high order methods. The difference of differential squares is one of the numerical methods in which the governing differential equations are converted into a group of first-order algebraic equations using the weight coefficients. In the differential quadratic difference method, the equations obtained at each stage with the help of Hamilton's principle are rewritten as follows [24]:

$$[M] \{\ddot{y}\} + [K] \{y\} = 0 \quad (35)$$

where  $[M]$  mass matrix,  $[K]$  stiffness matrix. The general solution is as follows:

$$y = \bar{y} e^{\omega t} \quad (36)$$

By inserting the relation (36) into the Eq.(35), the following equations are obtained (b: boundary, d: domain):

$$\begin{aligned} & \left( [M] \omega^2 + [K] \right) \{\bar{y}\} = 0 \\ & \mapsto \omega^2 \left( [M]_b \{y\}_b + [M]_d \{y\}_d \right) + \left( [K]_b \{y\}_b + [K]_d \{y\}_d \right) = 0 \end{aligned} \quad (37)$$

The equation of the boundary conditions is written as follows:

$$[B] \{y\} = 0 \mapsto [B]_b \{y\}_b + [B]_d \{y\}_d = 0 \mapsto \{y\}_b = -[B]_b^{-1} [B]_d \{y\}_d \quad (38)$$

$\{y\}_b$  is placed in Eqs. (37) as follows:

$$\begin{aligned} & \left( [M_m] \omega^2 + [K_m] \right) \{\bar{y}\} = 0 \\ & \rightarrow [M_m] = [M]_d - [M_m]_b [B]_b^{-1} [B]_d, \\ & \rightarrow [K_m] = [K]_d - [K_m]_b [B]_b^{-1} [B]_d, \end{aligned} \quad (39)$$

To solve the Eq. (39), the relation  $\{\dot{y}_d\} = \omega \{y_d\}$  is used, which is introduced by the name of the state space variable, and the relation is written as follows:

$$\omega [M_m] \{\dot{y}\} + [K_m] \{y\} = 0 \quad (40)$$

By dividing the whole expression by  $[M_m]$ , the following relationship is obtained:

$$\omega \{\dot{y}_d\} = -[M_m^{-1} K_m] \{y_d\} \quad (41)$$

Using the above relations, the state space equation is rewritten as follows:

$$\omega \begin{Bmatrix} y_d \\ \dot{y}_d \end{Bmatrix} = [A] \begin{Bmatrix} y_d \\ \dot{y}_d \end{Bmatrix} \rightarrow [A] = \begin{bmatrix} 0 & I \\ -M_m^{-1}K_m & 0 \end{bmatrix} \tag{42}$$

For beam theory in the present work, the first step to start solving is to use the following relations:

$$U(x,t) = U(x) e^{\omega\tau}, \quad W(x,t) = W(x) e^{\omega\tau}, \quad \phi(x,t) = \phi(x) e^{\omega\tau}, \tag{43}$$

where  $\omega$  represents the natural frequency. By applying the above relations to the set of motion equations, a standard vibrational motion equation is obtained and according to the above explanations are solved.

### 8 NUMERICAL RESULTS AND DISCUSSION

This paper has investigated the vibrations of three-layer composite beam. The upper and lower layers of the composite reinforced with graphene platelets are formed and three distribution models are considered for it according to the presented relationships. The middle layer is made up of porous materials.

Since the top layers are made of composite materials reinforced with graphene nanoplatelets and its mechanical properties are fix in all states that presented in as follow:

$$L = 1m, \quad \frac{h}{L} = 0.04, \quad \frac{h_c}{h} = 0.5, \quad \rho_c = 3500 \frac{kg}{m^3}, \quad E_M = 3GPa, \quad \nu_M = 0.34, \quad \rho_M = 1200 \frac{kg}{m^3},$$

$$E_{GPL} = 1.01TPa, \quad \nu_{GPL} = 0.186, \quad \rho_{GPL} = 1060 \frac{kg}{m^3}, \quad l_{GPL} = 2.5 \mu m, \quad w_{GPL} = 1.5 \mu m, \quad h_{GPL} = 1.5 nm,$$

And for porous matrial:  $e_m = 1 - \sqrt{1 - e_0}, \nu = 0.25, E = 60e9(Pa), \rho_m = 2700(Kg / m^3)$ , Chen et al. [25] studied the free and forced vibration behavior of FG porous Timoshenko beams with non-uniform porosity distribution (symmetric and asymmetric) using typical mechanical properties of an open-cell metal foam. Based on the Newmark- $\beta$  method the natural frequencies and transient dynamic deflections were obtained for porous beams and the effects of varying porosity distribution, porosity coefficient, and boundary condition were shown. Table 1 compare the present work with Ref. [25]. The results of this comparison show a good agreement (for  $\rho_m = 7850(Kg / m^3), E = 200GPa, \nu = 1/3$ ).

**Table 1**  
Comparison the results with Ref. [25]. Dimensionless fundamental frequencies of FG porous beams based on EBT ( $e_0=0.5$ ).

L/h	Symmetric porosity distribution			Nonsymmetric porosity distribution		
	Current Work (TBT)	Analytical	ANSYS	Current Work (TBT)	Analytical	ANSYS
H-H Beam						
10	0.2799	0.2798	0.2778	0.2600	0.2599	0.2549
20	0.1422	0.1422	0.1419	0.1318	0.1318	0.1296
50	0.0572	0.0571	0.0571	0.0530	0.0529	0.0521
C-C Beam						
10	0.5948	0.5944	0.6101	0.5476	0.5474	0.5600
20	0.3168	0.3166	0.3176	0.2889	0.2888	0.2941
50	0.1292	0.1291	0.1289	0.1175	0.1174	0.1183
C-H Beam						
10	0.4245	0.4242	0.4227	0.3900	0.3898	0.3905
20	0.2205	0.2203	0.2201	0.2014	0.2013	0.2015
50	0.092	0.0891	0.0891	0.0813	0.0813	0.0813
C-F Beam						
10	0.1009	0.1008	0.1007	0.0918	0.0917	0.0920
20	0.0508	0.0508	0.0508	0.0462	0.0462	0.0463
50	0.0204	0.0204	0.0204	0.0185	0.0185	0.0186

After deriving the equations with the help of 3 models of the beam and considering the 2 patterns in the porous layer, the frequency ( $\lambda = \omega L \sqrt{\rho_M} / \sqrt{E_M}$ ) changes in relation to parameters such as the thickness of the layers and the length of the beam, different vibrational modes ( $\lambda_1, \lambda_2, \lambda_3, \lambda_4$ ), porosity, of holes distribution pattern and mass fraction of graphene nanoplatelets are investigated. Figs. 3 to 8 and Tables 2 and 3 report these results.

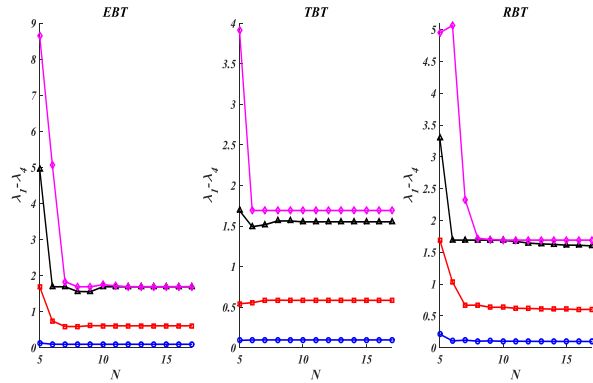


**Fig.3**  
Convergence.

In Fig.3, the convergence of the sandwich beam for the three theories of Reddy, Timoshenko and Euler is examined for the first four modes. In the DQ solution method, as it can be seen, by increasing the number of points in a certain interval, the beam frequency will be a certain value and will not change much. In this diagram, all modes have converged from point 10 onwards. The graphs are generally taken for the joint-girder boundary conditions and porosity distribution conditions of XX and porosity percentage of 0.5, except where noted.

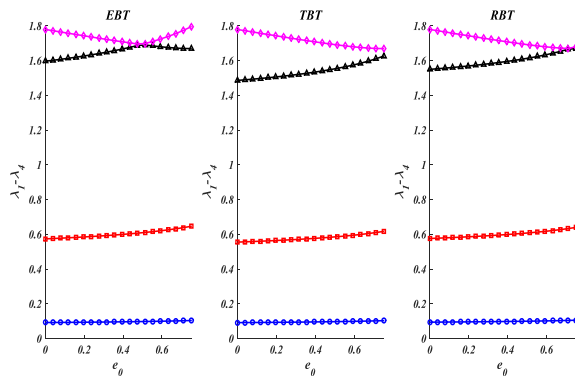


**Fig.4**  
The effect of porosity coefficient.

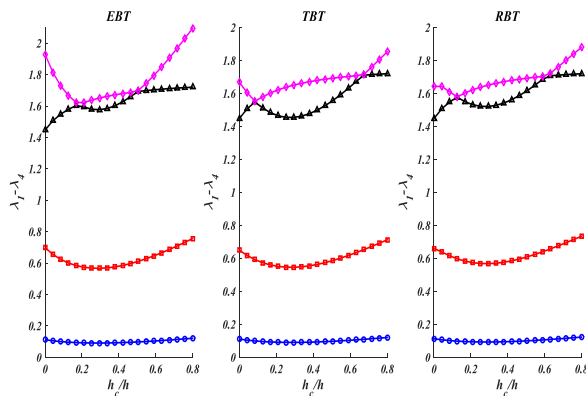
Fig. 4 shows the comparison of the frequency ratio for three modes of the beam theory based on the core porosity coefficient. Because in general increasing porosity decreases the stiffness to mass ratio and because of the direct relationship between this ratio and the natural frequency, therefore the frequency also decreases. Anyhow, the frequency in this structure increases with the increase of porosity because both the stiffness and the mass of the structure decrease in this porous structure, and the decrease in mass and density is greater than the decrease in the stiffness of the structure, so its overall ratio increases, and the frequency increases. In this case, porous materials can be used when the strength is not too high and the low weight of the structure is important.

Table 2 represents the effect of four mode changes on the natural frequency for the mentioned Porosity Distribution types. As shown in Fig. 4, with the increase of the porosity coefficient, the natural frequency decreases. This means that with the increase of porosity, the ratio of hardness to mass decreases, and due to the direct relationship of this ratio with the natural frequency, the frequency also decreases. In fact, increasing the porosity further reduces the stiffness and thus decreases the stiffness-to-mass ratio. It can also be seen that symmetrical and asymmetrical and then uniform distributions have the highest and lowest frequencies respectively in different modes. The frequencies were obtained based on material properties of the structures; comparing the result with previous studies shows that the frequency in uniform and nonsymmetric patterns are close that mainly depend on types of structure and material properties.

As mentioned, porous materials have less strength, but they greatly reduce the weight of the structure, so this decoration increases the use of the structure in many industries, including military and space. At the same time, by choosing different patterns of porous materials, it is possible to affect its vibration behavior in accordance with the use of the structure.

**Table 2**  
The effect of holes distribution pattern.

		Uniform	Symmetric	Non-symmetric
EBT	$\lambda_1$	0.0950	0.0975	0.0954
	$\lambda_2$	0.5938	0.6091	0.5963
	$\lambda_3$	1.6520	1.6920	1.6585
	$\lambda_4$	1.6750	1.6941	1.6923
TBT	$\lambda_1$	0.0944	0.0968	0.0948
	$\lambda_2$	0.5709	0.5849	0.5735
	$\lambda_3$	1.5178	1.5527	1.5259
	$\lambda_4$	1.6750	1.6920	1.6916
RBT	$\lambda_1$	0.0969	0.0994	0.0974
	$\lambda_2$	0.5932	0.6072	0.5957
	$\lambda_3$	1.5805	1.6130	1.5879
	$\lambda_4$	1.6750	1.6920	1.6920



**Fig.5**  
The effect of the thickness of the porous core.

The effect of the ratio of the thickness of the porous core to the total thickness in sandwich tires is shown in Fig. 5. Fig. 5 shows that the natural frequency increases significantly as the thickness of the core to the top increases from a ratio of 0.2 onwards. Accordingly, the total thickness remains constant, and the core thickness increases. As it is known, this increases the stiffness of the beam and also increases the stability of the beam. Therefore, the frequency increases. The figure has been revised for the first two frequencies to show the changes more accurately. The result shows that the geometry of the structure has a significant effect on its vibration behavior. Therefore, according to the type of behavior of the structure which can be seen from the diagrams, the geometry can be chosen according to the performance of the structure.

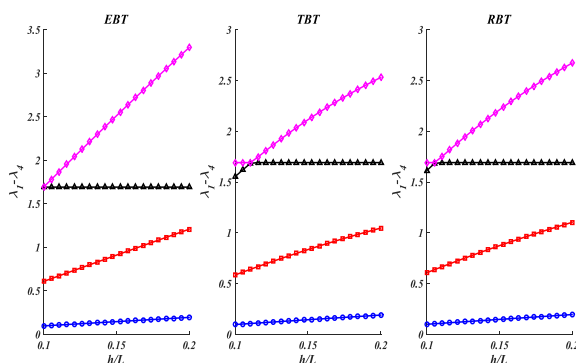


**Fig.6**  
The effect of the ratio of the thickness to the length of the beam.

Fig. 6 investigates the changes of the thickness of the entire beam to its length, as this ratio increases, the frequency also increases. It is noteworthy that the change in the thickness of the structure can change the order of the vibration modes, which can be seen in the third and fourth modes.

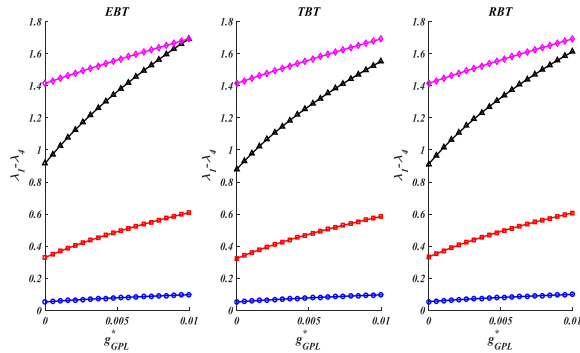


**Fig.7**  
The effect of mass fraction of graphene nanoplatelets.

Fig. 7 shows the effect of periodicity of the weight fraction of graphene nanoplatelets (GNPL) on the dimensionless frequency. This diagram is given for the uniform state, where the curves of this figure are fixed at the same numerical value of the GNPL weight fraction. According to the figure, it is proved that the frequency has a direct relationship with the weight fraction of GNPL, and with the increase of this value of the volume fraction, the frequency increases, and these changes are more visible in higher modes.

**Table 3**  
Effect of distribution pattern of graphene nanoplatelets.

		UU	XX	AA	AV	VA
EBT	$\lambda_1$	0.0619	0.0975	0.0562	0.0848	0.0209
	$\lambda_2$	0.3866	0.6091	0.3507	0.5301	0.1307
	$\lambda_3$	1.0753	1.6920	0.9740	1.4742	0.3634
	$\lambda_4$	1.4649	1.6941	1.4647	1.6053	0.7048
TBT	$\lambda_1$	0.0616	0.0968	0.0560	0.0843	0.0209
	$\lambda_2$	0.3775	0.5849	0.3436	0.5118	0.1298
	$\lambda_3$	1.0212	1.5527	0.9325	1.3673	0.3586
	$\lambda_4$	1.4649	1.6920	1.4640	1.6053	0.6900
RBT	$\lambda_1$	0.0638	0.0994	0.0580	0.0868	0.0214
	$\lambda_2$	0.3895	0.6072	0.3537	0.5308	0.1327
	$\lambda_3$	1.0610	1.6130	0.9667	1.4225	0.3649
	$\lambda_4$	1.4649	1.6920	1.4642	1.6053	0.6949

The information presented about the dimensionless frequency in Table 3 shows that mode effects and different types of GNPL distribution affect the frequency and stability of the structure. The highest frequency value corresponds to the fourth mode and distribution type FG-XX of the GNPL amplifier phase, which provides a more rigid structure. Table 3 shows that the distribution type XX, VA, where the reinforcing phase is placed more on the layer causes the stiffness of the structure and increases the stability of the structure. These frequency values in Reddy's theory are higher than Timoshenko's and Euler's theory.

Micromechanical analysis of composites has always been of special importance in terms of their performance. According to the results of this section, it can be determined how the increase or decrease of the reinforcements in the composite and how they are arranged affects the vibration frequency. And since the manufacturing processes in composites are diverse, the best way is chosen in terms of economy and performance.

### 9 CONCLUSIONS

In investigating the vibration behavior of a 3-layer beam consisting of a porous middle layer and upper and lower composite layers reinforced with graphene nanoplatelets, the following results are reported:

- ✓ The frequency increases with the increase of porosity because both the stiffness and the mass of the structure decrease.

- ✓ Increasing the porosity further reduces the stiffness and increase the frequency.
- ✓ Symmetrical and asymmetrical and then uniform distributions have the highest and lowest frequencies respectively.
- ✓ The natural frequency increases significantly as the thickness of the core to the top increases from a ratio of 0.2 onwards.
- ✓ As thickness of the entire beam to its length increases, the frequency also increases.
- ✓ The frequency has a direct relationship with the weight fraction of GNPL, and with the increase of this value of the volume fraction, the frequency increases.
- ✓ The highest frequency value corresponds to the distribution type FG-XX of the GNPL.
- ✓ These frequency values in Reddy's theory are higher than Timoshenko's and Euler's theory.

**APPENDIX A**

$$\begin{aligned}
 Q_{110} &= \int_z Q_{11}(z) dz, & I_0 &= \int_z \rho(z) dz, \\
 Q_{111} &= \int_z Q_{11}(z) z dz, & I_1 &= \int_z \rho(z) z dz, \\
 Q_{112} &= \int_z Q_{11}(z) z^2 dz, & I_2 &= \int_z \rho(z) z^2 dz
 \end{aligned}
 \tag{A.1}$$

$$\begin{aligned}
 Q_{110} &= \int_z Q_{11}(z) dz, & I_0 &= \int_z \rho(z) dz, \\
 Q_{111} &= \int_z Q_{11}(z) z dz, & I_1 &= \int_z \rho(z) z dz, \\
 Q_{112} &= \int_z Q_{11}(z) z^2 dz, & I_2 &= \int_z \rho(z) z^2 dz \\
 Q_{550} &= \int_z Q_{55}(z) dz
 \end{aligned}
 \tag{A.2}$$

$$\begin{aligned}
 Q_{110} &= \int_z Q_{11}(z) dz, & I_0 &= \int_z \rho(z) dz, \\
 Q_{111} &= \int_z Q_{11}(z) f(z) dz, & I_1 &= \int_z \rho(z) f(z) dz, \\
 Q_{112} &= \int_z Q_{11}(z) g(z) dz, & I_2 &= \int_z \rho(z) g(z) dz \\
 Q_{113} &= \int_z Q_{11}(z) f^2(z) dz, & I_3 &= \int_z \rho(z) f^2(z) dz, \\
 Q_{114} &= \int_z Q_{11}(z) f(z) g(z) dz, & I_4 &= \int_z \rho(z) f(z) g(z) dz, \\
 Q_{115} &= \int_z Q_{11}(z) g^2(z) dz, & I_5 &= \int_z \rho(z) g^2(z) dz \\
 Q_{550} &= \int_z Q_{55}(z) dz, & Q_{551} &= \int_z Q_{55}(z) \frac{df(z)}{dz} dz, \\
 Q_{552} &= \int_z Q_{55}(z) \frac{dg(z)}{dz} dz, & Q_{553} &= \int_z Q_{55}(z) \left(\frac{df(z)}{dz}\right)^2 dz, \\
 Q_{554} &= \int_z Q_{55}(z) \left(\frac{df(z)}{dz}\right) \left(\frac{dg(z)}{dz}\right) dz, & Q_{555} &= \int_z Q_{55}(z) \left(\frac{dg(z)}{dz}\right)^2 dz
 \end{aligned}
 \tag{A.3}$$

$$\begin{aligned}
 f(z) &= C_1 z^3 \\
 g(z) &= z - C_1 z^3 \\
 C_1 &= \frac{4}{3h^2}
 \end{aligned}$$

## REFERENCES

- [1] Ghorbanpour Arani A., Zarei M.S., 2015, Nonlocal vibration of Y-shaped CNT conveying nano-magnetic viscous fluid under magnetic field, *Ain Shams Engineering Journal* **6**(2): 565-575.
- [2] Choi J.D., Park S.B., Kim Y.K., 1993, Vibration characteristics of hollow cantilevered beams containing an electro-rheological fluid, *International Journal of Mechanical Sciences* **35**(9): 757-768.
- [3] Yeh J.Y., Chen L.W., Wang C.C., 2004, Dynamic stability of a sandwich beam with a constrained layer and electrorheological fluid core, *Composite Structures* **64**: 47-54.
- [4] Wei S., Meng K., Zhang G., Zhou W., 2007, Vibration characteristics of rotating sandwich beams filled with electrorheological fluids, *The Journal of Intelligent Materials Systems and Structures* **18**(11): 1165-1173.
- [5] Allahverdizadeh A., Mahjoob M.J., Maleki M., Nasrollahzadeh N., Naei M.H., 2013, Structural modeling, vibration analysis and optimal viscoelastic layer characterization of adaptive sandwich beams with electrorheological fluid core, *Mechanics Research Communications* **51**: 15-22.
- [6] Rezaeepazhand J., Pahlavan L., 2009, Transient response of sandwich beams with electrorheological core, *J The Journal of Intelligent Materials Systems and Structures* **20**(2): 171-179.
- [7] Ramkumar K., Ganesan N., 2009, Vibration and damping of composite sandwich box column with viscoelastic/electrorheological fluid core and performance comparison, *Materials and Design* **30**(8): 2981-2994.
- [8] Asgari M.A., Kouchakzadeh M., 2016, Acroclastic characteristics of magneto rheological fluid sandwich beams in supersonic airflow, *Composite Structures* **143**: 93-102.
- [9] Keshtegar B., Motezaker M., Kolahchi M., Nguyen-Thoi T., 2020, Wave propagation and vibration responses in porous smart nanocomposite sandwich beam resting on Kerr foundation considering structural damping, *Thin-Walled Structures* **154**: 106820.
- [10] Chen D., Kitipornchai S., Yang J., 2016, Nonlinear free vibration of shear deformable sandwich beam with a functionally graded porous core, *Thin-Walled Structures* **107**: 39-48.
- [11] Asemi K., Babaei M., Kiarasi F., 2020, Static natural frequency and dynamic analyses of functionally graded porous annular sector plates reinforced by graphene platelets, *Mechanics Based Design of Structures and Machines* **50**(11): 3853-3881.
- [12] Kiarasi F., Babaei M., Sarvi P., Asemi K., Hosseini M., Omidi Bidgoli M., 2021, A review on functionally graded porous structures reinforced by graphene platelets, *Journal of Computational Applied Mechanics* **52**(4): 731-750.
- [13] Kiarasi F., Babaei M., Mollaei S., Mohammadi M., Asemi K., 2021, Free vibration analysis of FG porous joined truncated conical-cylindrical shell reinforced by graphene platelets, *Advances in Nano Research* **11**(4): 361-380.
- [14] Babaei M., Asemi K., Kiarasi F., 2021, Dynamic analysis of functionally graded rotating thick truncated cone made of saturated porous materials, *Thin Walled Structures* **164**: 107852.
- [15] Rajamohan V., Sundararaman V., Govindarajan B., 2013, Finite element vibration analysis of a magnetorheological fluid sandwich beam, *Procedia Engineering* **64**: 603-612.
- [16] Amir S., Arshid E., Khoddami Maraghi Z., Loghman A., Ghorbanpour Arani A., 2020, Vibration analysis of magnetorheological fluid circular sandwich plates with magnetostrictive facesheets exposed to monotonic magnetic field located on visco-Pasternak substrate, *Journal of Vibration and Control* **26**(17-18): 1523-1537.
- [17] Zhong R., Wang Q., Ang J.T., Shuai C., Qin B., 2018, Vibration analysis of functionally graded carbon nanotube reinforced composites (FG-CNTRC) circular, annular and sector plates, *Composite Structures* **194**: 49-67.
- [18] Akhavan Alavi S.M., Mohammadimehr M., Edjtahed S.H., 2019, Active control of micro Reddy beam integrated with functionally graded nanocomposite sensor and actuator based on linear quadratic regulator method, *European Journal of Mechanics; A/Solids* **74**: 449-461.
- [19] Yue Y.M., Xu K.Y., Chen T., 2016, A micro scale Timoshenko beam model for piezoelectricity with flexoelectricity and surface effects, *Composite Structures* **136**: 278-286.
- [20] Ghorbanpour Arani A., Zamani M.H., 2018, Nonlocal free vibration analysis of FG-Porous shear and normal deformable sandwich nanoplate with piezoelectric face sheets resting on silica aerogel foundation, *Arabian Journal for Science and Engineering* **43**(9): 4675-4688.
- [21] Amir S., 2019, Orthotropic patterns of visco-Pasternak foundation in nonlocal vibration of orthotropic graphene sheet under thermo-magnetic fields based on new first-order shear deformation theory, *Proceedings of the Institution of Mechanical Engineers, Part L: Journal of Materials: Design and Applications* **233**(2): 197-208.
- [22] Sahmani S., Safaei B., 2021, Large-amplitude oscillations of composite conical nanoshells with in-plane heterogeneity including surface stress effect, *Applied Mathematical Modelling* **89**: 1792-1813.
- [23] Yeh L., Chen J.Y., 2004, Vibration of a sandwich plate with a constrained layer and electrorheological fluid core, *Composite Structures* **65**(2): 251-258.
- [24] Asemi, S.R., 2014, Influence of initial stress on the vibration of double-piezoelectric-nanoplate systems with various boundary conditions using DQM, *Physica E: Low-Dimensional Systems and Nanostructures* **63**: 169-179.
- [25] Yeh L., Chen J.Y., 2004, Free and forced vibrations of shear deformable functionally graded porous beams, *International Journal of Mechanical Sciences* **108-109**: 14-22.